

This is an electronic reprint of the original article. This reprint may differ from the original in pagination and typographic detail.

---

## Asymmetric ionic aerogel of biologic nanofibrils for harvesting electricity from moisture

Yang, Weiqing; Li, Xiankai; Han, Xiao; Zhang, Weihua; Wang, Zengbin; Ma, Xiaomei; Li, Mingjie; Li, Chaoxu

*Published in:*  
Nano Energy

*DOI:*  
[10.1016/j.nanoen.2020.104610](https://doi.org/10.1016/j.nanoen.2020.104610)

Published: 14/02/2020

*Document Version*  
Final published version

*Document License*  
CC BY-NC-ND

[Link to publication](#)

*Please cite the original version:*

Yang, W., Li, X., Han, X., Zhang, W., Wang, Z., Ma, X., Li, M., & Li, C. (2020). Asymmetric ionic aerogel of biologic nanofibrils for harvesting electricity from moisture. *Nano Energy*, 71, Article 104610. <https://doi.org/10.1016/j.nanoen.2020.104610>

### General rights

Copyright and moral rights for the publications made accessible in the public portal are retained by the authors and/or other copyright owners and it is a condition of accessing publications that users recognise and abide by the legal requirements associated with these rights.

### Take down policy

If you believe that this document breaches copyright please contact us providing details, and we will remove access to the work immediately and investigate your claim.

1 **Asymmetric Ionic Aerogel of Biologic Nanofibrils for Harvesting Electricity from Moisture**

2 *Weiying Yang,<sup>a</sup> Xiankai Li,<sup>b,c</sup> Xiao Han,<sup>b,c</sup> Weihua Zhang,<sup>d</sup> Zengbin Wang,<sup>b</sup> Xiaomei Ma,<sup>\*a</sup> Mingjie*

3 *Li<sup>\*b,c</sup> and Chaoxu Li,<sup>\*b,c</sup>*

4 <sup>a</sup>College of Chemistry and Chemical Engineering, Qingdao University, 308 Ningxia Road, Qingdao,  
5 Shandong 266071, P. R. China

6 <sup>b</sup>Group of Biomimetic Smart Materials, Qingdao Institute of Bioenergy and Bioprocess Technology,  
7 Chinese Academy of Sciences, Songling Road 189, Qingdao 266101, P. R. China

8 <sup>c</sup>Center of Material and Optoelectronics Engineering, University of Chinese Academy of Sciences,  
9 19A Yuquan Road, Beijing 100049, P. R. China

10 <sup>d</sup>Johan Gadolin Process Chemistry Centre, c/o Laboratory of Wood and Paper Chemistry, Åbo  
11 Akademi University, Turku FI-20500, Finland

12 \*Corresponding authors: Xiaomei M ([mxm@qdu.edu.cn](mailto:mxm@qdu.edu.cn)), Mingjie Li ([limj@qibebt.ac.cn](mailto:limj@qibebt.ac.cn)) and Chaoxu  
13 Li ([licx@qibebt.ac.cn](mailto:licx@qibebt.ac.cn))

14

15 **Abstract**

16 Artificial asymmetric ionic membranes have attracted great interests in harvesting electricity from  
17 ubiquitous water activities, while mostly based on delicately-designed nanopores/nanochannels, either  
18 to harness saline water in mimic of cytomembranes or to harness moisture with carbon nanomaterials.  
19 Herein, fully biological asymmetric ionic aerogels were fabricated from biological oppositely-charged  
20 nanofibrils through a facile freeze-casting method. When exposing to moisture, these nanofibrils may  
21 be hydrated by capturing moisture and thus simulate the charged nanochannels for ion transport. Ion  
22 dissociation and diffusion ions would induce directional movement of charges, thereby leading to a  
23 potential up to 115 mV. With sustainability, biocompatibility and biodegradability, these biological  
24 nanogenerators may promise a low-cost and high-efficiency electricity harvest strategy from moist air,  
25 being capable of serving as self-powered wearable, biomedical and miniaturized electronic devices.

26 **Keywords:** Asymmetric ionic aerogel; Biological nanofibrils; Electricity harvest; Moisture.

27

## 28 **1. Introduction**

29 Porous Janus membranes, i.e., porous membranes with asymmetric properties (e.g., chemical  
30 compositions, wettability, charges and porosity) on each side, have shown great potential in various  
31 energy-efficient applications (e.g., emulsification [1], demulsification [2], fog harvesting [3] and  
32 energy harvesting [4]), because of their super capabilities of reducing permeating resistance of specific  
33 gases and liquids, and further allowing their selective mass transport. In particular, asymmetric surface  
34 charges of porous membranes, which enable selective permeation of anions or cations in mimic of cell  
35 membranes [5, 6], have been implemented in electrodialysis [7], ionic rectification [8], and  
36 nanofiltration of charged nanomaterials [9], *etc* [10, 11]. Besides these, asymmetric ionic membranes  
37 have also shown great superiority in harvesting electricity from ubiquitous waters (e.g., salinity  
38 gradient [12] and moisture [13]) for applications in flexible, wearable and biomedical devices.  
39 However, in most cases these asymmetric ionic membranes were based on the delicately-designed  
40 nanopores/nanochannels (e.g., made of anodic aluminum oxide (AAO) [12, 14], block copolymers [4],  
41 closely packing particles [15] and graphene [13]). Owing to uncontrollable and broad-range nanopores  
42 sizes, biological fibrous membranes, despite having broad applications in filtration/separation  
43 membranes [16, 17], have rarely been endeavored to serve as asymmetric ionic membranes, especially  
44 for the purpose of harvesting energy for water activities (e.g., evaporation, diffusion and flow).

45 Within a charged nanopore/nanochannel with its radius comparable to the Debye length of the  
46 ionic solution, its surface charges would produce an electric double layer, and then influence both the  
47 enrichment and transport of anions and cations [18]. In order to avoid the possible presence of ionic  
48 concentration polarization for selective and efficient ion transport, asymmetric ionic channels were  
49 normally introduced to optimize the ion-enrichment and ion-depletion effects [19]. For example,

50 anion/cation diode-like selective transport was achieved by asymmetric ionic nanochannel membranes  
51 of polyimide [20], polyamide [21], polyethylene terephthalate (PET) [22] and closely packing silica  
52 nanoparticles [15]. Ionic rectification with the ratio up to hundreds was obtained with asymmetric  
53 conical PET nanochannel with opposite surface charge [23]. Electricity was also harvested from  
54 salinity gradient and osmotic energy of saline water, based on asymmetric ionic channels of AAO [12,  
55 14], block copolymers [4], and mesoporous carbon [12].

56 Besides harvesting energy from saline water, asymmetric ionic membranes could also be  
57 employed to harvest electricity from moisture. In contrast to saline water, moisture from industry,  
58 natural evaporation and physiological processes (e.g., transpiration and respiration) is more ubiquitous  
59 and spontaneous in the environment, and thus capable of affording a huger application potential for  
60 facile and low-cost electricity generation. In most cases, the asymmetric ionic membranes were  
61 produced from carbon nanomaterials (e.g., graphene oxides) with a gradient distribution of charged  
62 groups (e.g., carboxyl) [13, 24-27]. When exposing to moisture, adsorption and condensation of  
63 moisture occurred within the inner pores of nanomaterials [13, 24, 25, 28-30]. Ions (e.g.,  $H^+$  and  $H_3O^+$ )  
64 may be dissociated with a concentration gradient, and thus generate a transmembrane electric pulse  
65 [13, 25, 26, 29, 30]. Notably, electric potential arising from waterflow would also be possible during  
66 this process, according to the mechanisms of stream potential [31, 32], electron drag [33], ion hopping  
67 [34], polarization-induced-dissociation effect [35], and charge exchange between water molecules and  
68 carbon nanomaterials [36].

69 In order to relieve environmental/cytotoxic concerns for wide use of high-cost inorganic/carbon  
70 nanomaterials [28, 37, 38], sustainable biomaterials have attracted great interests in harvesting energy  
71 from water activities [39]. In particular, we found that biological nanofibrils (NFs) with charged

72 surfaces may be hydrated in moisture and serve equivalently as the charged nanochannels for energy  
73 harvest from moist air flow [40]. With comparison to inorganic nanomaterials and synthetic polymers  
74 [41, 42], biologic nanomaterials have the advantages of abundant functional groups and facileness of  
75 chemical modification. Thus, in this study asymmetric ionic aerogel was produced from 2,2,6,6-  
76 tetramethylpiperidine-1-oxyl-oxidized cellulosic NFs (i.e., TEMPO-CNFs) and quaternized cellulosic  
77 NFs (i.e., Quatern-CNFs) in a facile directional-freeze casting method. When exposed to moist air, the  
78 asymmetric ionic aerogel could induce an open circuit potential ( $V_{oc}$ ) as high as ~115 mV with a  
79 maximum short circuit current ( $I_{sc}$ ) of 45 nA, which is a comparable or superior overall performance  
80 compared with reported moisture-driven generators (see details in Table S1). This production strategy  
81 also maintained valid for other types of biological nanofibrils with oppositely charged states, such as  
82 amyloid fibrils of bovine serum albumin (BSA)/chitin NFs, carboxylated silk NFs/chitin NFs, BSA  
83 NFs/lysozyme NFs, TEMPO-CNFs/chitin NFs and TEMPO-CNFs/lysozyme NFs.

84 With comparison to the asymmetric ionic nanopores/channels reported in the literature, biological  
85 nanofibrils were not only sustainable and low-cost, but also promising to avoid complicated procedures  
86 for nanochannel production and surface treatment (e.g., plasma, laser and harsh oxidation). Their facile  
87 procedures of surface chemical modification also ensured to produce asymmetric membranes with  
88 opposite charges on each side, in contrast to gradient distributions of charges groups in asymmetric  
89 ionic membranes of graphene oxides [13]. Thus, in addition to harvesting electricity from moist air  
90 flow by using mono-component aerogels of biological nanofibrils [40], electricity could also be  
91 harvested directly from more ubiquitous moist air through this bilayer type of asymmetric ionic aerogel,  
92 which may promise a low-cost and high-efficiency handy power supply solution, and facilitate wide  
93 applications of innovative self-powered electronic devices.

## 94 **2. Experimental section**

### 95 *2.1 Fabrication of asymmetric ionic aerogel*

96 Fabrication of silk NFs, amyloid NFs, deacetylated chitin NFs and BSA NFs was detailed in  
97 Supporting Information. Aerogels were fabricated with the suspensions of these NFs. Typically, a  
98 suspension of Quatern-CNFs (0.3–0.6 wt%) was poured into a mold, followed by subjecting to  
99 unidirectional freezing with liquid nitrogen. Unidirectional freezing was also performed after pouring  
100 another solution of Tempo-CNFs (0.3–0.6 wt%). The asymmetric bilayer aerogel (2–10 mm in  
101 thickness) was obtained by freeze-drying in a freeze drier (FD-1C-50, Beijing BoYiKang) at  $-55\text{ }^{\circ}\text{C}$ .  
102 The aerogel was laminated between two electrodes of Pt nets (purchased from Global Jinxin  
103 International Technology Co., LTD , with the mesh size of 0.25 mm and diameter of Pt wires of 0.1  
104 mm) with the size =  $3 \times 3$ ,  $4 \times 4$  or  $5 \times 5\text{ cm}^2$ , serving as the current collectors (see details in Fig. S5).  
105 The RH value was adjusted by saturated salt solutions within the enclosed environment at  $25\text{ }^{\circ}\text{C}$ , such  
106 as RH=99% ( $\text{Na}_2\text{HPO}_4$ ), RH=90% ( $\text{Na}_2\text{CO}_3$ ), RH=80% ( $\text{NH}_4\text{Cl}$ ), RH=70% ( $\text{CO}(\text{NH}_2)_2$ ), RH=60%  
107 ( $\text{NaBr}$ ) and RH=50% ( $\text{Ca}(\text{NO}_3)_2$ ).

### 108 *2.2 Sensing measurements*

109 The sensors were constructed by laminating the bilayer aerogel (diameter of 2 cm, thickness of 6 mm  
110 and ratio of bilayer thickness of  $\sim 1$ ) within the Pt electrodes. For finger sensing, the sensor was fixed  
111 on a glass slide. And an index finger slowly approached to the sensor at ambient RH. Both the electric  
112 potential ( $V_{\text{oc}}$ ) and the distance between the sensor and finger were measured simultaneously. For  
113 breath sensing, the sensor was integrated to a commercial aspirator (3M N95), the  $V_{\text{oc}}$  variation was  
114 recorded under strenuous exercise and relaxation states. For humidity sensing, the sensor was fixed on  
115 one hydroponic *Alocasia genus* outdoors (Qingdao in North China: East longitude  $\sim 120^{\circ}$  and North

116 latitude  $\sim 36^\circ$ ). The  $V_{oc}$  value was recorded from 8 o'clock to 20 o'clock (Apr. 26th, 2019), together  
117 with the temperature, RH and solar density.

### 118 *2.3 Characterization*

119 Transmission electron microscopy (TEM) and field emission scanning electron microscopy (FESEM)  
120 were performed on Hitachi H-7650 (Hitachi, Japan) and JEOL 7401 (JEOL, Japan), respectively. Zeta  
121 potential was recorded on Zetasizer Nano ZSE (Malvern Instruments Ltd., England). Elemental  
122 analysis was carried out on an Elementar Analysensysteme GmbH Vario EL Cube elemental analyser.  
123 Open circuit voltage and resistance in real time were recorded using a digital multimeter (MS8265,  
124 Mastech Ltd. Dongguan, China). Short-circuit current is recorded in real time using a digital nanometer  
125 (JX-A04, Jianxin Ltd. Dongguan, China). Relative humidity values were measured by a digital RH  
126 meter (S-WS05, Shenxinhui Electronics Co., Ltd. Shenzhen, China).

## 127 **3. Results and discussion**

### 128 *3.1 Design of asymmetric ionic nanofibrous aerogel as biological generator*

129 Bio-macromolecules and their assemblies are characteristic of abundant functional groups and hereby  
130 opt to be chemically modified for different surface charges and charge densities [43-45]. Being one of  
131 the most fundamental building blocks of natural biomaterials, biological NFs with negative or positive  
132 surface charges could be extracted from naturally abundant biomass and/or synthesized through  
133 supramolecular self-assembly (Fig. 1a-1c & Fig. S1-S2) [40, 46]. For instance, CNFs with negative  
134 and positive charges were exfoliated mechanically from hardwood via TEMPO-mediated oxidization  
135 (i.e., TEMPO-CNFs) [47] and 2,3-epoxypropyl trimethylammonium chloride cationization (i.e.,  
136 Quatern-CNFs) [48], respectively (Fig. 1a-1d); Negatively charged silk NFs (i.e., carboxylated silk  
137 NFs) were exfoliated mechanically from *Bombyx mori* cocoons through a NaClO oxidization method

138 (Fig. S2) [49]; And positively charged amyloid NFs were synthesized via supramolecular assembly of  
139 lysozyme at pH  $\sim$ 2 and 60 °C (i.e., lysozyme NFs) (Fig. S2) [50]. Negatively charged amyloid NFs  
140 were synthesized via a poor-solvent-induced fibrillation of BSA molecules (i.e., BSA NFs) (Fig. S2)  
141 [49]. All these NFs had the diameter of  $<10$  nm and the aspect ratio of  $>10^2$  (Fig. 1b & Fig. S1-S2).  
142 Among these biological NFs, charged CNFs have been studied in details, because they are one type of  
143 the most abundant biological materials in nature, and have seen diverse applications in catalysts,  
144 electro-optical films, nanofiber-reinforced composites, microelectronics, *etc* [45, 51]. Their surface  
145 charge densities and  $\zeta$ -potential could be tuned precisely, e.g., 0.5~1.39 mmol g<sup>-1</sup> carboxyl groups and  
146 -25~-43 mV of  $\zeta$ -potential for TEMPO-CNFs, and 0.5~1.28 mmol g<sup>-1</sup> quaternary ammonium groups  
147 and 30~54 mV of  $\zeta$ -potential for Quatern-CNFs (Fig. S1).

148 Owing to their highly charged surfaces, these CNFs ( $\sim 3.5$  mg mL<sup>-1</sup>) maintained colloiddally stable  
149 at the nematic states (inset of Fig. 1b). After directionally freezing the dispersion of TEMPO-CNFs  
150 with liquid nitrogen, another layer of Quatern-CNFs dispersion was casted onto its top. Then fibrous  
151 bi-layered aerogel with oriented structure was produced through a freeze-drying process (Fig. 1e &  
152 S3). Hierarchical porosities were further revealed with the oriented microscale pores (i.e., the channel  
153 width 1–10  $\mu$ m) and nanoscale pores (i.e., the size  $<100$  nm). The aerogel porosity varied within  
154 99.2–99.6% by tuning the CNFs concentrations in their dispersions from 3 to 6 mg ml<sup>-1</sup> (Fig. S4).

155 The humidity-induced nanogenerator was constructed by laminating the bilayer of cellulosic  
156 aerogel (e.g., 3/3 mm/mm thick for TEMPO-CNFs/Quatern-CNFs; 2 cm in diameter) between two  
157 parallel Pt nets as current collectors (mesh size  $\sim 0.25$  mm) (Fig. 1e-1f & S5). At an environmental  
158 relative humidity (RH) of  $\sim 99\%$ ,  $V_{oc}$  increased dramatically to a maximum value as high as  $\sim 115$  mV  
159 at  $\sim 20$  min, and then decreased gradually to vanishment within  $\sim 30$  min (Fig. 1g). With alternately

160 switching moisture between On and Off, a variational period of  $V_{oc}$  was observed. This power  
161 generation ability could be cyclically repeated without severe decay (Fig. 1g & S6). In addition, an  $I_{sc}$   
162 up to 45 nA was also aroused by the moisture, following the variation route similar to that of  $V_{oc}$  (Fig.  
163 S6 & S7).

### 164 3.2 Suggested mechanism of the biological generator

165 Further investigation showed that low RH (e.g., <50%) produced negligible  $V_{oc}$ , while the higher RH  
166  $\geq 50\%$  promoted the  $V_{oc}$  value progressively up to maximum value of  $\sim 115$  mV at RH  $\sim 99\%$  (Fig. 2a  
167 & S8). These phenomena confirmed that water played a vital role in this electricity-generation process.  
168 To be noted, biological NFs not only had the ultrathin diameter of  $< 10$  nm and large specific surface  
169 area, but also had the contents of hydrophilic groups (e.g., hydroxy, carboxyl in TEMPO-CNFs and  
170 quaternary ammonium in Quatern-CNFs) higher than those of carbon nanomaterials used for moisture-  
171 induced electricity generation [13, 24, 25, 28, 29]. When exposing to moist air, these fibrous aerogels  
172 could easily capture moisture and immobilize water molecules via hydrogen bonding (e.g., TEMPO-  
173 CNFs-O $\cdots$ H-OH and Quatern-CNFs-N $\cdots$ H-OH). And inevitably capillary condensation occurred  
174 within the nanoscale pores of the aerogel according to Kelvin's equation [52]:

$$175 \quad \ln \frac{P}{P_0} \sim \frac{\gamma}{r} \quad (1)$$

176 where  $P_0$  and  $P$  are the saturation vapor pressures of water near planar surface and concave meniscus,  
177 respectively;  $r$  is the curvature radius of the water surface (being negative for concave meniscus); and  
178  $\gamma$  is the surface tension of water. For the bilayer aerogel with the hydrophilic group concentration of  
179  $\sim 0.9$  mmol  $g^{-1}$  (i.e., TEMPO-CNFs with the carboxyl content of  $\sim 0.89$  mmol  $g^{-1}$  and Quatern-CNFs  
180 with the quaternary ammonium group of  $\sim 0.91$  mmol  $g^{-1}$ , and thickness ratio of 1), the moisture uptake  
181 capacity increased dramatically with the increasing RH, and got a maximum value up to  $\sim 0.9$  g  $g^{-1}$

182 (Fig. 2b & S9). And thus a bilayer hydrated shell would form on the surfaces of these NFs: an inner  
 183 layer with immobilized water molecules and an out layer with free water molecules (Fig. 2d). Polar  
 184 groups of the CNFs could release a large amount of counter ions (e.g.,  $H^+$ ,  $Na^+$  and  $Cl^-$ ), and built an  
 185 electric double layer (EDL) [36, 53]. Therefore, an ion conductive network would form within the  
 186 hydrated surface and channels of the fibrous aerogels [54]. Correspondingly, the internal resistance  
 187 sharply decreased from  $\sim 100$  to  $0.8\text{ M}\Omega$  when RH increased from 55 to 99% (Fig. 2b).

188 Due to the bilayer structure of the aerogel, cations were mainly produced within the TEMPO-CNF  
 189 aerogel layer, while anions were produced mainly within the Quatern-CNF aerogel layer. Driven by  
 190 the osmotic pressure, directional movement of net charges induced the potential (i.e.,  $V_{oc}$ ). And the  
 191 consumption of the free ions osmosis and net charge transfer led to an evanescent  $V_{oc}$  (Fig. 2c). When  
 192 switched to a depressed RH (RH <10%) the released ions would go back to the surfaces of NFs, and  
 193 thereby produced a recyclable  $V_{oc}$  generation under “On/Off” moisture stimuli (Fig. 1f).

### 194 3.3 Structural optimization of asymmetric ionic aerogel nanogenerator

195 Besides the RH value, the content of charged groups on biological NFs can also play a prominent role  
 196 in the device performance.  $V_{oc}$  increased obviously with an increasing concentration of charged groups  
 197 as exhibited in Fig. 3a. According to Nernst equation for a concentration difference cell [55]:

$$198 \quad V \sim \frac{RT}{F} \left( \left| \ln \frac{a_2^+}{a_1^+} \right| + \left| \ln \frac{a_2^-}{a_1^-} \right| \right) \quad (2)$$

199 where the R, T and F represent the gas constant, temperature and Faraday’s constant;  $a_2^+$  and  $a_1^+$   
 200 refer to the activities of cations in the Quatern-CNFs side and interface of the two sides, respectively,  
 201 while  $a_2^-$  and  $a_1^-$  refer to the activities of anions in the TEMPO-CNFs side and interface of the two  
 202 sides, respectively. Thus, more dissociable groups would increase the number of counter ions, and thus  
 203 enhance the output voltage. However, the aerogels with excessive dissociable groups (e.g., >1 mmol

204  $\text{g}^{-1}$ ) led to a slight decrease in  $V_{\text{oc}}$  at high RH values (e.g., 99%) (Fig. 3a), due to the structural collapse  
205 under hydration (Fig. S10).

206 The  $V_{\text{oc}}$  value could also be tuned by the geometric structures of the fibrous aerogels (Fig. 3b-3e).  
207 A larger device area seemingly led to a higher  $I_{\text{sc}}$  value (Fig. 3c). With the constant device thickness  
208 (i.e., 6 mm) and dissociable group contents (e.g.,  $\sim 0.9 \text{ mmol g}^{-1}$  for carboxyl groups in TEMPO-CNFs  
209 and quaternary ammonium in Quatern-CNFs), the thickness ratio of the bilayer was optimal at  $\sim 1:1$ ,  
210 owing to the nearly equal amounts of free charges. Thus the aerogel generator could be optimized with  
211 the porosity of  $\sim 99.3\%$ , the aerogel thickness of  $\sim 6 \text{ mm}$ , and the bilayer thickness ratio of  $\sim 1:1$  (Fig. 3b-  
212 3e). Furthermore, these nanogenerators could also be connected in series or in parallel for high  $V_{\text{oc}}$  or  
213  $I_{\text{sc}}$  (Fig. 3f & Fig. S11).

#### 214 *3.4 Electricity-generation performance of asymmetric ionic aerogel nanogenerator*

215 The electricity generated by this biological diode generator could be conveniently accumulated and  
216 stored with the conventional solutions. As shown in Fig. 4a, commercial capacitors (e.g., capacitance  
217 3.3 mF) were charged with the diode generator, being able to serve as power supply for daily  
218 appliances such as lighting a red LED with a driven voltage  $\sim 1.5 \text{ V}$  (Fig. S12 & Video S1). Since  
219 moisture widely exists in nature (e.g., evaporation of waters and transpiration of plants) and in industry  
220 (e.g., drying and water cooling), the biological nanogenerators enable a variety of applications. For  
221 instance, the generator was capable of a self-powered electrical humidity sensor with a sensitivity as  
222 high as  $2.35 \text{ mV/RH}\%$  (Fig. 4b), being superior to most of the humidity sensors in the literature, such  
223 as porous carbon humidity sensor ( $\sim 2 \text{ mV/RH}\%$ ), polymer nanowire sensor ( $\sim 1.3 \text{ mV/RH}\%$ ),  
224 graphene oxide hydrovoltaic sensor ( $\sim 0.7\text{--}1 \text{ mV/RH}\%$ ), graphene oxide/poly(sodium 4-  
225 styrenesulfonate) composite dielectric sensor ( $0.0375 \text{ mV/RH}\%$ ) and polyaniline piezoresistive sensor

226 (0.64 mV/RH%) [24, 25, 27, 41, 56, 57]. Because of the distance-determined moisture distribution  
227 near the human skin, the generator could also detect the distance away from the skin, which may  
228 promise diverse applications like touchless control and contact warning (Fig. 4c & Fig. S13) [58].

229 The biological nanogenerator could also be powered by some physiological processes, e.g.,  
230 transpiration and perspiration, rendering huge potentials for self-powered health monitoring devices.  
231 When integrated with a commercial respirator (like 3M N95), the generator could detect the dynamic  
232 characteristics of breathing (e.g., frequency and intensity). As shown in Fig. 4d, the frequency of the  
233  $V_{oc}$  pulses coincided with the breath before and after strenuous exercise with a breathing frequency of  
234 20 and 38  $\text{min}^{-1}$ . Moreover, this biologic generator could also be installed near plants to monitor and  
235 quantify their transpiration process which releases >99% of water consumed by plants into air [59]. As  
236 shown in Fig. 4e & S14, the electrical signal of this generator above one hydroponic *Alocasia genus*  
237 was collected on daytime of Apr. 26 th, 2019 (Qingdao in North China: East longitude  $\sim 120^\circ$  and  
238 North latitude  $\sim 36^\circ$ ), which reflected the intensity of plant transpiration in real time. Furthermore, the  
239 biological generator could be fully degraded in natural soil leachate within 25 days (Fig. S15), once  
240 again demonstrating the nanogenerator ideal for next generation wearable electronic devices.

#### 241 **4. Conclusion**

242 In this study, asymmetric ionic aerogels of biological NFs enabled the electric energy harvest from  
243 moisture variation. Biological NFs were not only sustainable and low-cost, but also promising in  
244 abundant functional groups and facileness of chemical modification. Asymmetric ionic aerogels were  
245 fabricated of carboxylated and quaternized cellulosic NFs through a facile directional-freeze casting  
246 method. When exposing the asymmetric aerogels to moisture, these NFs could capture water from air  
247 and formed ion conductive networks with hydrated nanochannels. Ion dissociation and diffusion would

248 lead to directional movement of charges, thereby producing a potential across the aerogel. The  
249 generators of asymmetric ionic aerogels could also be fabricated by other biological NFs pairs such as  
250 BSA NFs/deacetylated chitin NFs, carboxylated silk NFs/deacetylated chitin NFs, BSA NFs/lysozyme  
251 NFs, TEMPO-CNFs/deacetylated chitin NFs and TEMPO-CNFs/lysozyme NFs (Fig. S16).  
252 Combining sustainability, biocompatibility and biodegradability, these biological nanogenerators may  
253 promise a low-cost and high-efficiency handy power supply strategy, as well as capable of serving as  
254 self-powered wearable, biomedical and miniature electronic devices.

## 255 **Acknowledgements**

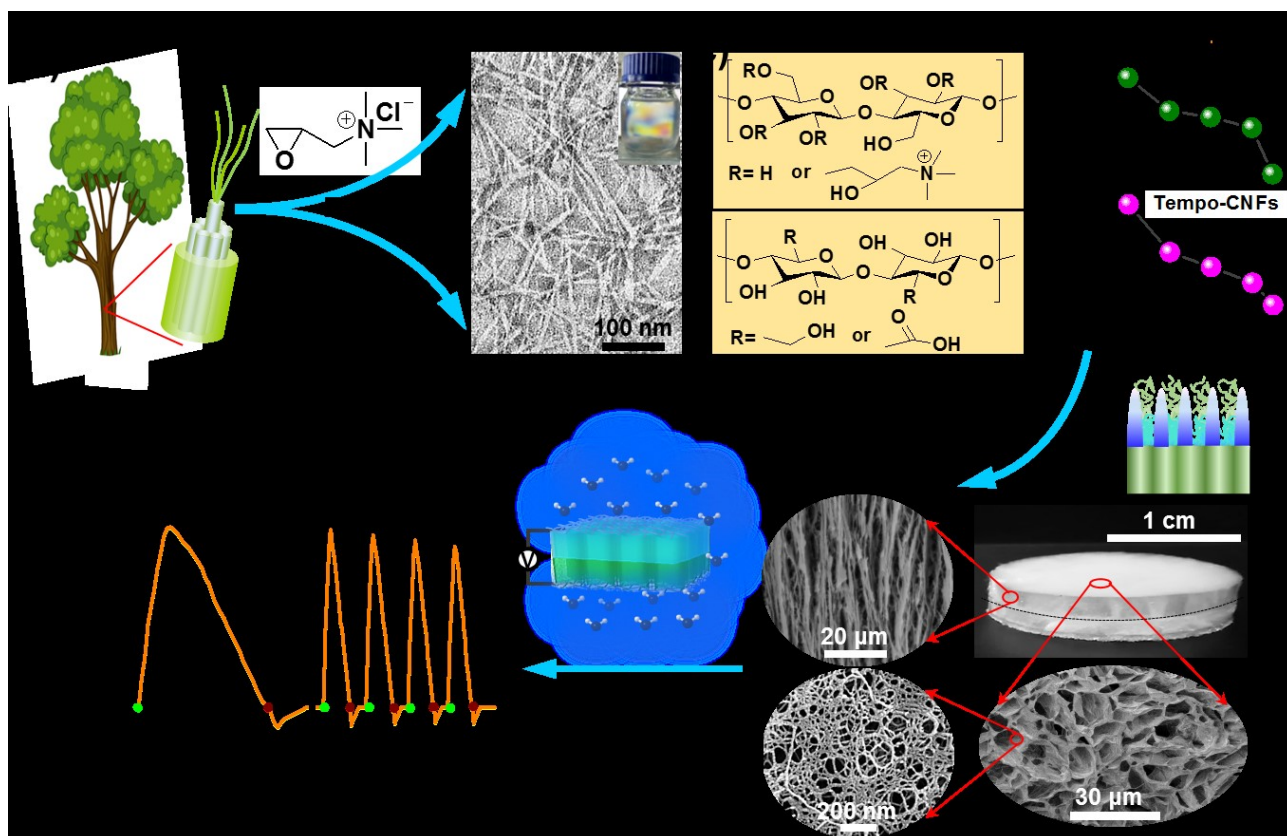
256 National Natural Science Foundation of China (No. 21474125 and 51608509), Chinese “1000 Youth  
257 Talent Program”, Shandong “Taishan Youth Scholar Program”, Shandong Provincial Natural Science  
258 Foundation (No. JQ201609), “135” Projects Fund of CAS QIBEBT Director Innovation Foundation  
259 and Shandong Collaborative Innovation Centre for Marine Biomass Fibre Materials and Textiles are  
260 kindly acknowledged for financial support.

## 261 **References**

- 262 [1] Z. Wang, Y. Wang, G. Liu, *Angew. Chem. Int. Ed.*, 55 (2016) 1291–1294.  
263 [2] Z. Wang, M. Lehtinen, G. Liu, *Angew. Chem. Int. Ed.*, 56 (2017) 12892–12897.  
264 [3] P. Zhang, B. Peng, J. Wang, L. Jiang, *Adv. Funct. Mater.*, 29 (2019) 1904535.  
265 [4] Z. Zhang, X. Sui, P. Li, G. Xie, X.-Y. Kong, K. Xiao, L. Gao, L. Wen, L. Jiang, *J. Am. Chem. Soc.*,  
266 139 (2017) 8905–8914.  
267 [5] P. Jin, D. Bulkley, Y. Guo, W. Zhang, Z. Guo, W. Huynh, S. Wu, S. Meltzer, T. Cheng, L.Y. Jan,  
268 *Nature*, 547 (2017) 118–122.  
269 [6] G. Eric, M. Roderick, *Science*, 310 (2005) 1461–1465.  
270 [7] D.A. Vermaas, M. Saakes, K. Nijmeijer, *Energy Environ. Sci.*, 45 (2011) 7089–7095.  
271 [8] Z. Zhang, X.Y. Kong, K. Xiao, G. Xie, Q. Liu, Y. Tian, H. Zhang, J. Ma, L. Wen, L. Jiang, *Adv.*  
272 *Mater.*, 28 (2016) 144–150.  
273 [9] J. Liu, D. Hua, Y. Zhang, S. Japip, T.S. Chung, *Adv. Mater.*, 30 (2018) 1705933.  
274 [10] G. Wei, T. Ye, J. Lei, *Acc Chem Res*, 46 (2013) 2834–2846.  
275 [11] A. van den Berg, H.G. Craighead, P. Yang, *Chem. Soc. Rev.*, 39 (2010) 899–900.  
276 [12] J. Gao, W. Guo, D. Feng, H. Wang, D. Zhao, L. Jiang, *J. Am. Chem. Soc.*, 136 (2014)  
277 12265–12272.

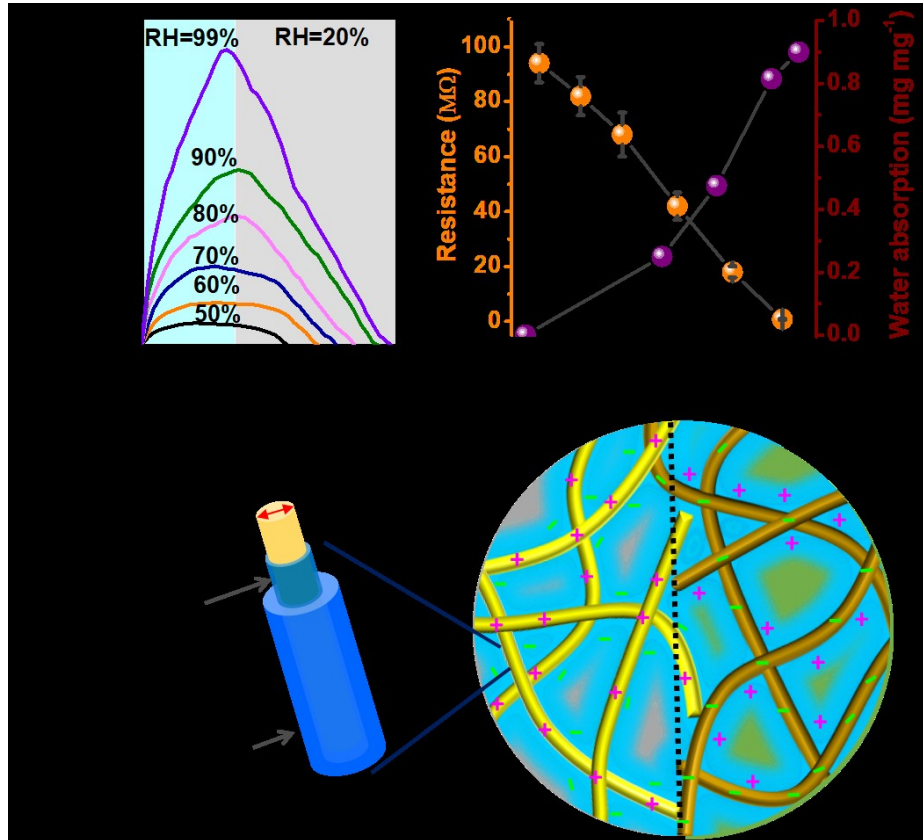
- 278 [13] F. Zhao, Y. Liang, H. Cheng, L. Jiang, L. Qu, *Energy Environ. Sci.*, 9 (2016) 912–916.
- 279 [14] W. Xin, Z. Zhang, X. Huang, Y. Hu, T. Zhou, C. Zhu, X.-Y. Kong, L. Jiang, L. Wen, *Nat. Commun.*,  
280 10 (2019) 3876.
- 281 [15] E. Choi, C. Wang, G.T. Chang, J. Park, *Nano Lett.*, 16 (2016) 2189–2197.
- 282 [16] Z. Wang, J. Xu, M. Li, C. Su, X. Wu, Y. Zhang, J. You, C. Li, *ACS Appl. Mater. Interfaces*, 11  
283 (2019) 8576–8583.
- 284 [17] Y. Wang, L. Zhu, J. You, F. Chen, Z. Lu, X. Yan, C. Li, Y. Wang, L. Zhu, J. You, *ACS Sustainable*  
285 *Chem. Eng.*, 5 (2017) 10673–10681.
- 286 [18] H.C. Yang, Y. Xie, J. Hou, A.K. Cheetham, V. Chen, S.B. Darling, *Adv. Mater.*, 30 (2018) 1801495.
- 287 [19] Z. Zhang, L. Wen, L. Jiang, *Chem. Soc. Rev.*, 47 (2018) 322–356.
- 288 [20] Q. Liu, K. Xiao, L. Wen, Y. Dong, G. Xie, Z. Zhang, Z. Bo, L. Jiang, *ACS Nano*, 8 (2014)  
289 12292–12299.
- 290 [21] F. Li, Z. Zhou, *Small*, 14 (2018) 1702961.
- 291 [22] M. Liu, H. Zhang, K. Li, L. Heng, S. Wang, Y. Tian, L. Jiang, *Adv. Funct. Mater.*, 25 (2015)  
292 421–426.
- 293 [23] I. Vlassioux, Z.S. Siwy, *Nano Lett.*, 7 (2007) 552.
- 294 [24] K. Liu, P. Yang, S. Li, J. Li, T. Ding, G. Xue, Q. Chen, G. Feng, J. Zhou, *Angew. Chem., Int. Ed.*,  
295 55 (2016) 8003–8007.
- 296 [25] Z. Fei, C. Huhu, Z. Zhipan, J. Lan, Q. Liangti, *Adv. Mater.*, 27 (2015) 4351–4357.
- 297 [26] C. Yang, Y. Huang, H. Cheng, L. Jiang, L. Qu, *Adv. Mater.*, 31 (2019) 1805705.
- 298 [27] H. Cheng, Y. Huang, L. Qu, Q. Cheng, G. Shi, L. Jiang, *Nano Energy*, 45 (2018) 37–43.
- 299 [28] D. Shen, M. Xiao, G. Zou, L. Liu, W.W. Duley, Y.N. Zhou, *Adv. Mater.*, 30 (2018) 1705925.
- 300 [29] K. Hu, R. Xiong, H. Guo, R. Ma, S. Zhang, Z.L. Wang, V.V. Tsukruk, *Adv. Mater.*, 28 (2016)  
301 3549–3556.
- 302 [30] T. Xu, X. Ding, C. Shao, L. Song, T. Lin, X. Gao, J. Xue, Z. Zhang, L. Qu, *Small*, (2018) 1704473.
- 303 [31] F.H. Van der Heyden, D.J. Bonthuis, D. Stein, C. Meyer, C. Dekker, *Nano Lett.*, 6 (2006)  
304 2232–2237.
- 305 [32] F.H. van der Heyden, D. Stein, C. Dekker, *Phys. Rev. Lett.*, 95 (2005) 116104.
- 306 [33] P. Král, M. Shapiro, *Phys. Rev. Lett.*, 86 (2001) 131–134.
- 307 [34] J. Yin, Z. Zhang, X. Li, J. Zhou, W. Guo, *Nano Lett.*, 12 (2012) 1736–1741.
- 308 [35] S. He, Y. Zhang, L. Qiu, L. Zhang, E.H. Sargent, *Adv. Mater.*, 30 (2018) 1707635.
- 309 [36] G. Xue, Y. Xu, T. Ding, J. Li, J. Yin, W. Fei, Y. Cao, J. Yu, L. Yuan, L. Gong, J. Chen, S. Deng, J.  
310 Zhou, W. Guo, *Nature Nanotechnology*, 12 (2017) 317–321.
- 311 [37] Z. Zhang, X. Li, J. Yin, Y. Xu, W. Fei, M. Xue, Q. Wang, J. Zhou, W. Guo, *Nat. nanotechnol.*, 13  
312 (2018) 1109–1119.
- 313 [38] Y. Xu, P. Chen, H. Peng, *Chem.-Eur. J.*, 24 (2018) 6287–6294.
- 314 [39] X. Gao, T. Xu, C. Shao, Y. Han, B. Lu, Z. Zhang, L. Qu, *Journal of Materials Chemistry A*, 7  
315 (2019) 20574–20578.
- 316 [40] M. Li, L. Zong, W. Yang, X. Li, J. You, X. Wu, Z. Li, C. Li, *Adv. Funct. Mater.*, (2019) 1901798.
- 317 [41] X. Nie, B. Ji, N. Chen, Y. Liang, Q. Han, L. Qu, *Nano Energy*, 46 (2018) 297–304.
- 318 [42] T. Xu, X. Ding, Y. Huang, C. Shao, L. Song, X. Gao, Z. Zhang, L. Qu, *Energy Environ. Sci.*, 12  
319 (2019) 972–978.
- 320 [43] M. Krishnan, N. Mojarad, P. Kukura, V. Sandoghdar, *Nature*, 467 (2010) 692–695.
- 321 [44] B.E. Cohen, T.B. McAnaney, E.S. Park, Y.N. Jan, S.G. Boxer, L.Y. Jan, *Science*, 296 (2002)

322 1700–1703.  
323 [45] S. Ling, W. Chen, Y. Fan, K. Zheng, K. Jin, H. Yu, M.J. Buehler, D.L. Kaplan, *Prog. Polym. Sci.*,  
324 85 (2018) 1–56.  
325 [46] X. Wu, X. Han, L. Lv, M. Li, J. You, C. Li, *J. Colloid Interface Sci.*, 527 (2018) 117–123.  
326 [47] T. Saito, Y. Nishiyama, J.-L. Putaux, M. Vignon, A. Isogai, *Biomacromolecules*, 7 (2006)  
327 1687–1691.  
328 [48] A. Olszewska, P. Eronen, L.-S. Johansson, J.-M. Malho, M. Ankerfors, T. Lindstrom, J.  
329 Ruokolainen, J. Laine, M. Osterberg, *Cellulose*, 18 (2011) 1213–1226.  
330 [49] K. Zheng, J. Zhong, Z. Qi, S. Ling, D.L. Kaplan, *Adv. Funct. Mater.*, 28 (2018) 1806380.  
331 [50] J. You, M. Li, B. Ding, X. Wu, C. Li, J. You, M. Li, B. Ding, X. Wu, C. Li, *Adv. Mater.*, 29 (2017)  
332 1606895.  
333 [51] L. Zhu, L. Zong, X. Wu, M. Li, H. Wang, J. You, C. Li, *ACS Nano*, 12 (2018) 4462–4468.  
334 [52] S. Siboni, *Am. J. Phys.*, 74 (2006) 565–568.  
335 [53] K. Uetani, H. Yano, *Biomacromolecules*, 12 (2010) 348–353.  
336 [54] J. Peng, D. Cao, Z. He, J. Guo, P. Hapala, R. Ma, B. Cheng, J. Chen, W.J. Xie, X.-Z. Li, *Nature*,  
337 557 (2018) 701–705.  
338 [55] W. Di, *Advanced Materials Technologies*, 4 (2016) 1600145.  
339 [56] H.-W. Yu, H.K. Kim, T. Kim, K.M. Bae, S.M. Seo, J.-M. Kim, T.J. Kang, Y.H. Kim, *ACS Appl.*  
340 *Mater. Interfaces*, 6 (2014) 8320–8326.  
341 [57] S.J. Patil, A. Adhikari, M.S. Baghini, V.R. Rao, *Sensor Actuat. B: Chem*, 203 (2014) 165–173.  
342 [58] J. Feng, L. Peng, C. Wu, X. Sun, S. Hu, C. Lin, J. Dai, J. Yang, Y. Xie, *Adv. Mater.*, 24 (2012)  
343 1969–1974.  
344 [59] J.M. Baker, C.H.M.V. Bavel, *Plant Cell Environ.*, 10 (2010) 777–782.  
345  
346



347  
 348 **Fig. 1.** Synthesis pathway of asymmetric ionic nanofibrous aerogel as biological generator. (a)  
 349 Schematic illustration of synthesizing oppositely charged CNFs from wood via mechanical exfoliation.  
 350 (b) Typical TEM image of negatively charged TEMPO-CNFs. (c-d) Chemical structures (c) and Zeta  
 351 potentials (d) of Quatern-CNFs (top) and TEMPO-CNFs (bottom). (e) Optical and SEM images of  
 352 asymmetric ionic aerogel fabricated by directional freezing and freeze drying. (f)  $V_{oc}$  generated with  
 353 asymmetric ionic generator under periodic moist stimuli. RH = 99%.

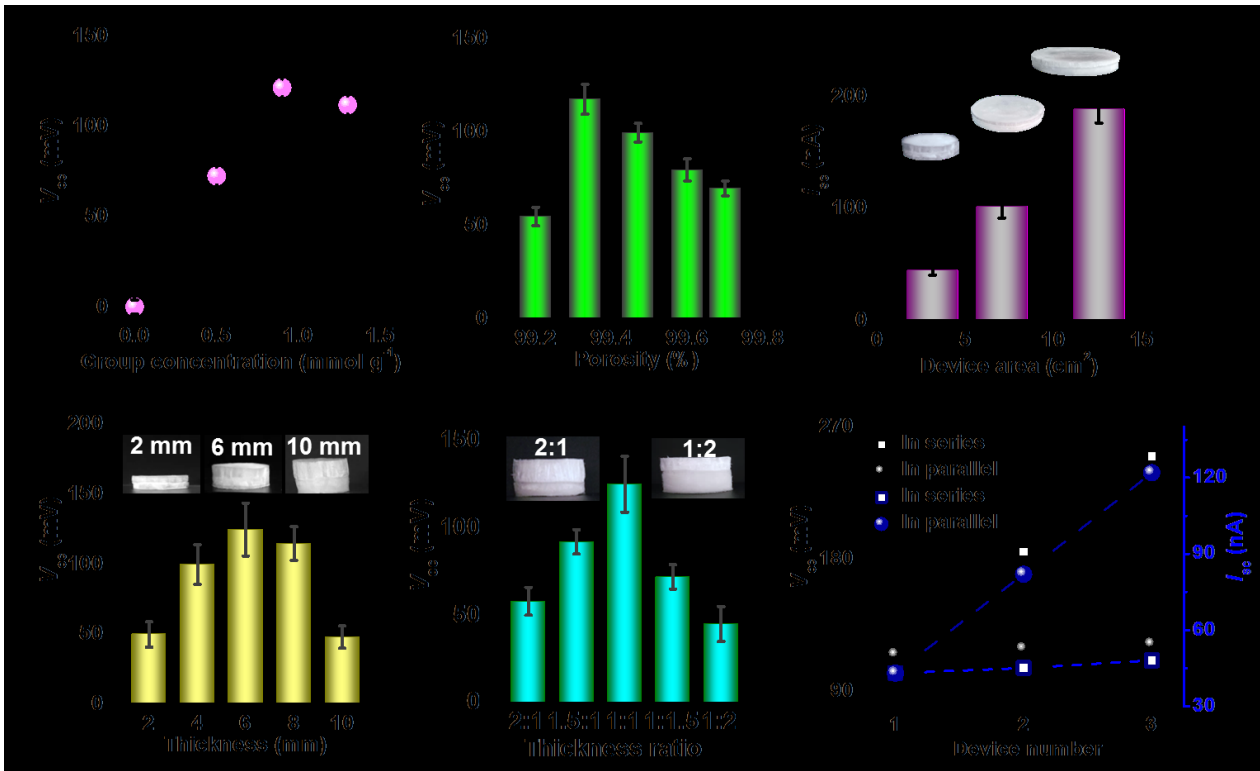
354



355

356 **Fig. 2.** Electricity-generation mechanism of asymmetric ionic aerogel. (a)  $V_{oc}$  variation upon exposing  
 357 to different RHs. (b) Capacity of water absorption and internal resistance at different RHs. Carboxyl  
 358 content of TEMPO-CNFs:  $\sim 0.89\ mmol\ g^{-1}$ ; Quaternary ammonium group of Quatern-CNFs:  $\sim 0.91$   
 359  $mmol\ g^{-1}$ . Generator diameter: 2 cm; Thickness: 6 mm; Bilayer thickness ratio:  $\sim 1$ ; RH=99%. (c)  
 360 Schematic illustration of voltage induced by directional movement and neutralization of free ions  
 361 within hydrated charged nanochannels.

362



363

364

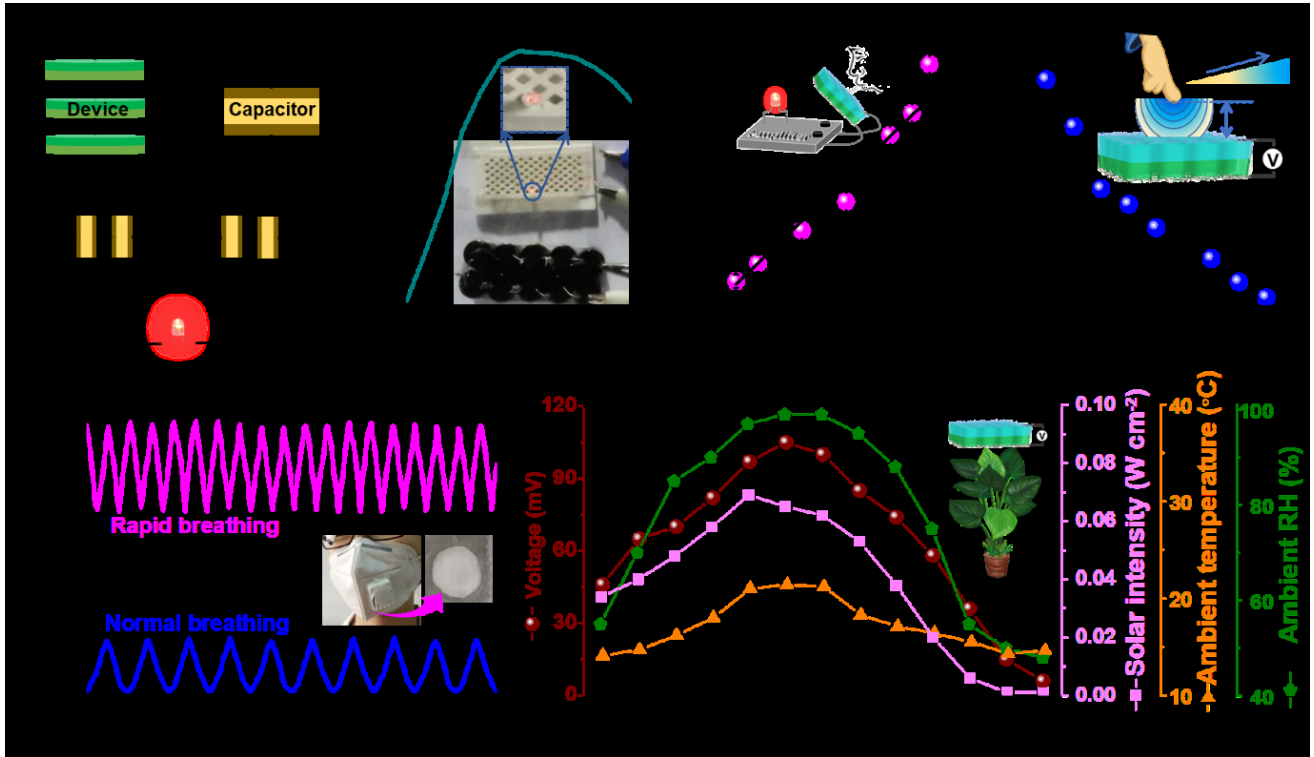
365

366

367

368

**Fig. 3.** Structural optimization of asymmetric ionic aerogel nanogenerator. (a) Effect of charged group content on equilibrium  $V_{oc}$ . (b) Effect of aerogel porosity on  $V_{oc}$ . (c) Effect of aerogel area on  $V_{oc}$ . (d) Effect of aerogel thickness on  $V_{oc}$ . (e) Effect of thickness ratio of TEMPO-CNFs/Quatern-CNFs layers on  $V_{oc}$ . (f)  $V_{oc}$  and  $I_{sc}$  of generators in series and parallel. Generator diameter: 2 cm; Thickness: 6 mm; Thickness ratio: ~1; RH =99%.



369

370 **Fig. 4.** Electricity-generation performance of asymmetric ionic aerogel nanogenerator. (a) Charging  
 371 commercial capacitors with biological generator in series and parallel (Left) and discharging curve  
 372 (Right). The inset shows a commercial red LED was powered by capacitors. (b) Asymmetric ionic  
 373 aerogel nanogenerator serving as electrical humidity sensor. (c) Asymmetric ionic aerogel  
 374 nanogenerator to sense finger distance. (d)  $V_{oc}$  variation when exposing to respiration (N, Frequency)  
 375 settled on commercial aspirator. (e)  $V_{oc}$  variation when exposing to transpiration hanged above an  
 376 *Alocasia macrorrhiza* at natural conditions (Beijing Time 8-20 o'clock, Qingdao in North China,  
 377 Daytime on Apr. 26th, 2019). Generator diameter: 2 cm; Thickness: 6 mm; Thickness ratio: ~1.